

Optimizing thermodynamic cycles with two finite-sized reservoirs

Hong Yuan,¹ Yu-Han Ma^{1,*} and C. P. Sun^{1,2,†}

¹Graduate School of China Academy of Engineering Physics, Number 10 Xibeiwang East Road, Haidian District, Beijing 100193, China

²Beijing Computational Science Research Center, Beijing 100193, China

 (Received 4 August 2021; revised 30 November 2021; accepted 1 February 2022; published 16 February 2022)

We study the nonequilibrium thermodynamics of a heat engine operating between two finite-sized reservoirs with well-defined temperatures. Within the linear response regime, it is found that the uniform temperature of the two reservoirs at final time τ is bounded from below by the entropy production $\sigma_{\min} \propto 1/\tau$. We discover a general power-efficiency tradeoff depending on the ratio of heat capacities (γ) of the reservoirs for the engine, and a universal efficiency at maximum average power of the engine for arbitrary γ is obtained. For practical purposes, the operation protocol of an ideal gas heat engine to achieve the optimal performance associated with σ_{\min} is demonstrated. Our findings can be used to develop a general optimization scenario for thermodynamic cycles with finite-sized reservoirs in real-world circumstances.

DOI: [10.1103/PhysRevE.105.L022101](https://doi.org/10.1103/PhysRevE.105.L022101)

Introduction. Thermodynamic constraints exist in all kinds of energy-conversion machines. Among these constraints, Carnot efficiency serves as the upper bound for efficiency of heat engines. Such a bound is only achieved by reversible thermodynamic cycles under the quasistatic limit [1], and is therefore not tight for practical heat engines with finite cycle time. Considering the restriction of operation time, abundant tighter thermodynamic constraints were obtained for finite-time thermodynamic cycles [2–6], for example, the efficiency at maximum power [7–17], tradeoff relation between power and efficiency [18–23], and thermodynamic uncertainty relation [24,25]. In particular, the power-efficiency tradeoff determines the feasible operation regime for finite-time heat engines and has attracted considerable attention.

Recently, to deal with another practicality that the heat is basically stored by a finite amount of material with finite heat capacity, the finiteness of the reservoir size is also taken into account as a physical restriction on thermodynamic cycles [26–33]. This issue is crucial for responding to the increasingly severe energy crisis with limited material resources, and the efficiency at maximum work (EMW) [26,28,33,34] and efficiency at maximum average power (EMAP) [27,29,30,33] were proposed as typical thermodynamic constraints in this case.

As two fundamental restrictions in energy conversion processes, the finiteness of operation time and reservoir size usually coexist in real-world circumstances. Hence, a more practical question naturally arises: Is there a power-efficiency tradeoff associated with finite-sized reservoirs? In this Letter, we address this question by studying the finite-time performance of a linear irreversible heat engine operating between two finite-sized reservoirs. We discover a general tradeoff relation between power and efficiency, and a universal EMAP

is obtained. Furthermore, we find the optimal operation of the engine to achieve the boundary of the tradeoff.

Minimum entropy production and the uniform temperature. As illustrated in Fig. 1, we consider a linear irreversible heat engine operating between a hot reservoir with initial temperature $T_h^{[i]}$ and a cold reservoir with initial temperature $T_c^{[i]}$. Both of these two reservoirs are of finite size with the heat capacity C_h and C_c , respectively. As follows, we focus on the case of constant heat capacity $C_{h(c)}$. From the initial time $t = 0$, the engine converts the heat to work consecutively through a control parameter λ until the two reservoirs finally reach the thermal equilibrium state at $t = \tau$ with a uniform temperature $T_c^{[f]} = T_h^{[f]} \equiv \tilde{T}$. Here, we stress that the heat capacity of at least one reservoir needs to be finite, otherwise the temperatures of the two reservoirs will always maintain their initial values instead of reaching the same within finite time. In the following, we adopt the assumptions used in Refs. [29,30,33].

(i) Both of the two reservoirs relax rapidly such that they are always in the quasiequilibrium states with time-dependent temperatures $T_h(t)$ and $T_c(t)$.

(ii) The total operation time τ (macrotime scale) is much larger than the cycle time τ_c (microtime scale, treated as a unit of time hereafter), and hence the engine undergoes sufficiently many cycles, namely, $M \equiv \tau/\tau_c \gg 1$, before it stops operating.

The entropy production rate reads $\dot{\sigma} = -\dot{Q}_h/T_h + \dot{Q}_c/T_c$, where $\dot{Q}_h = -C_h\dot{T}_h$ represents the heat absorption from the hot reservoir to the engine of a cycle, and $\dot{Q}_c = C_c\dot{T}_c$ is the heat release from the engine to the cold reservoir of a cycle. As a result, the total entropy production $\sigma(\tau) \equiv \int_0^\tau \dot{\sigma} dt$ is

$$\sigma(\tau) = C_c \ln \frac{\tilde{T}}{T_c^{[i]}} + C_h \ln \frac{\tilde{T}}{T_h^{[i]}}. \quad (1)$$

The uniform temperature \tilde{T} is thus determined by the entropy production as

$$\tilde{T} = \tilde{T}(\sigma) = [T_h^{[i]}]^{1/\gamma+1} [T_c^{[i]}]^{1/\gamma+1} \exp \left[\frac{\sigma}{C_h + C_c} \right], \quad (2)$$

*yhma@gscaep.ac.cn

†suncp@gscaep.ac.cn

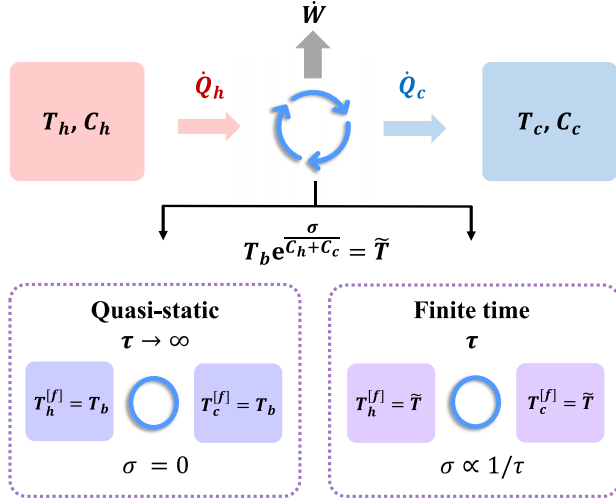


FIG. 1. Demonstration of a heat engine operating between two finite-sized heat reservoirs. The heat engine operates between a finite-sized hot (cold) reservoir with initial temperature $T_h^{[i]}$ ($T_c^{[i]}$). The heat engine stops working when the two reservoirs reach the final uniform temperature $T_c^{[f]} = T_h^{[f]} \equiv \tilde{T}$. C_c (C_h) denotes the heat capacity of the cold (hot) reservoir. The increase in entropy production σ will increase the final temperature \tilde{T} [Eq. (2)].

namely, the uniform temperature rises as the entropy production increases. Here the heat capacity ratio $\gamma \equiv C_c/C_h$ quantifies the asymmetry in size of the reservoirs. $T_b \equiv \tilde{T}(\sigma = 0)$ is the final temperature in the reversible case with no entropy production. The reversible case is discussed in the Supplemental Material (SM) [35].

Then, we exploit the linear irreversible thermodynamics to obtain $\sigma(\tau)$ as well as \tilde{T} explicitly in the finite-time regime. Under the tight-coupling condition $q \equiv L_{21}/\sqrt{L_{11}L_{22}} = 1$, the entropy production rate reads [29,30]

$$\dot{\sigma} = \frac{\dot{Q}_h^2}{L_{22}} = \frac{C_h^2 \dot{T}_h^2}{L_{22}}, \quad (3)$$

where L_{ij} ($i, j = 1, 2$) is the Onsager coefficient, and L_{22} corresponds to the thermal conductivity [36–38]. The adopted tight-coupling condition can be practical realized, e.g., by a finite-time ideal gas Carnot engine [36].

The Cauchy-Schwarz inequality

$$\left[\int_0^\tau (\sqrt{\dot{\sigma}})^2 dt \right] \left(\int_0^\tau dt \right) \geq \left(\int_0^\tau \sqrt{\dot{\sigma}} dt \right)^2 \quad (4)$$

implies that the entropy production $\sigma(\tau) = \int_0^\tau \dot{\sigma} dt = \int_0^\tau (\sqrt{\dot{\sigma}})^2 dt$ has a lower bound, namely [35],

$$\sigma(\tau) \geq \frac{\Sigma_{\min}}{\tau} \equiv \sigma_{\min}. \quad (5)$$

In this inequality, only the first order of τ^{-1} is kept in the long-time regime [16], and the equal sign is saturated with constant entropy production rate, i.e., $\dot{\sigma} = \Sigma_{\min}/\tau^2$ ($\dot{Q}_h = \sqrt{L_{22}\Sigma_{\min}}/\tau$). The minimum dissipation coefficient $\Sigma_{\min} \equiv (\int_{T_h^{[i]}}^{T_b} C_h dT_h / \sqrt{L_{22}})^2$, characterizing how irreversible entropy production increases away from the reversible regime, is a τ -independent dissipation coefficient. Generally, Σ_{\min} depends

on the specific form of L_{22} and relates to the thermodynamic length [38–41]. In the simplest case with constant L_{22} , $\Sigma_{\min} = C_h^2 [T_h^{[i]} - T_b]^2 / L_{22}$. The typical $1/\tau$ scaling of irreversibility shown in Eq. (5) has also been discovered in the finite-time isothermal processes [13,23,42–44].

We remark here that although the minimum entropy production σ_{\min} in Eq. (5) is obtained with the tight-coupling condition, σ_{\min} actually serves as the overall lower bound for entropy production σ with arbitrary q . This is because σ decreases monotonically with the increase of $|q|$ (see SM [35] for strict proof). Therefore, for general cases within the linear response regime, the uniform temperature is bounded from below by the minimal entropy production as $\tilde{T} \geq \tilde{T}(\sigma_{\min})$.

Tradeoff between power and efficiency. The work output in the whole process is $W(\tau) = Q_h(\tau) - Q_c(\tau)$, where $Q_h(\tau) = C_h(T_h^{[i]} - \tilde{T})$ and $Q_c(\tau) = C_c(\tilde{T} - T_c^{[i]})$. The maximum extractable work $W_{\max} \equiv \lim_{\sigma \rightarrow 0} W(\tau)$ [35] is achieved in the reversible case. Note that $W(\tau)$ is a monotonically decreasing function of \tilde{T} [35], which indicates that, referring to Eq. (2), the entropy production will reduce $W(\tau)$ in comparison with W_{\max} . In this sense, we define the finite-time dissipative work:

$$W_d \equiv W_{\max} - W(\tau) = (C_h + C_c)(\tilde{T} - T_b). \quad (6)$$

It follows from Eqs. (2), (5), and (6) that the constraint on dissipative work is explicitly obtained as $W_d \geq T_b \Sigma_{\min} / \tau \equiv W_d^{(\min)}$ [35]. In terms of W_d , the efficiency in the finite-time case, $\eta \equiv W(\tau)/Q_h(\tau)$, reads

$$\eta = \frac{W_{\max} - W_d}{W_{\max}/\eta_{\text{MW}} - W_d/(1 + \gamma)}, \quad (7)$$

where the EMW $\eta_{\text{MW}} = \eta_{\text{MW}}(\gamma)$ reads [35]

$$\eta_{\text{MW}} \equiv 1 - \gamma \left[\frac{\eta_C}{1 - (1 - \eta_C)^{\gamma/(\gamma+1)}} - 1 \right] \quad (8)$$

and is achieved in the reversible case [33], and $\eta_C \equiv 1 - T_c^{[i]}/T_h^{[i]}$ is the Carnot efficiency determined by the initial temperatures of the reservoirs.

Expressing W_d in terms of η according to Eq. (7), the constraint on dissipative work ($W_d \geq W_d^{(\min)}$) becomes

$$W_d = \frac{W_{\max}(\eta_{\text{MW}} - \eta)}{\eta_{\text{MW}}[1 - \eta/(1 + \gamma)]} \geq \frac{T_b \Sigma_{\min}}{\tau}. \quad (9)$$

Eliminating the duration τ in this inequality with the average power $P \equiv W(\tau)/\tau$ of the whole process, we find the tradeoff relation between power and efficiency [35]:

$$\tilde{P} \leq \frac{4\lambda\tilde{\eta}(1 - \tilde{\eta})}{(\lambda\tilde{\eta} + 1 - \tilde{\eta})^2}. \quad (10)$$

Here, $\lambda \equiv 1 - \eta_{\text{MW}}/(1 + \gamma)$, $\tilde{P} \equiv P/P_{\max}$, $\tilde{\eta} \equiv \eta/\eta_{\text{MW}}$, and $P_{\max} \equiv W_{\max}^2/(4T_b \Sigma_{\min})$ is the maximum average power. As the main result of this paper, the above relation specifies the complete optimization regime for the heat engines operating between finite-sized reservoirs. The equal sign of Eq. (10) is achieved with the minimum entropy generation σ_{\min} , which determines the optimal performance of the heat engine, namely, the maximum power for a given efficiency. The optimal operation of the heat engine will be discussed later. We emphasize that such a tradeoff constrains the performance of all the heat engines operating in the linear response

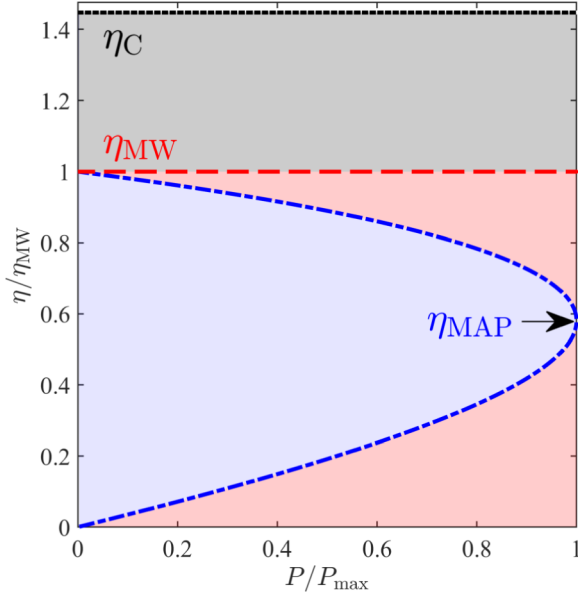


FIG. 2. “Phase diagram” $\tilde{P} - \tilde{\eta}$ of the heat engine performance between finite reservoirs. The blue dash-dotted curve and the (light blue) area therein represent the tradeoff between $\tilde{P} = P/P_{\max}$ and $\tilde{\eta} = \eta/\eta_{\text{MW}}$ in Eq. (10). P_{\max} is the maximum average power. The efficiency at maximum work η_{MW} in Eq. (8) is plotted with the red dashed line, while the corresponding Carnot efficiency $\eta_{\text{C}} = 0.8$ is plotted with the black dotted line. In this example, we use $\gamma = C_c/C_h = 1$.

regime, because σ_{\min} is the overall lower bound for irreversibility as we remarked below Eq. (5).

In the symmetric case with $\gamma = 1$ (see SM [35] for the asymmetric cases with $\gamma = 0.01, 100$), the power-efficiency tradeoff is illustrated in Fig. 2 with the blue dash-dotted curve and the (light blue) area therein. The efficiency corresponding to the maximum power ($\tilde{P} = 1$) is denoted as η_{MAP} in this figure, and will be detailed in the following. $\eta_{\text{C}} = 0.8$ is used in this plot. Due to the finiteness of the heat reservoirs, the (gray) area between efficiency at maximum work η_{MW} (red dashed line) and Carnot efficiency η_{C} (black dotted line) becomes a forbidden regime in the “phase diagram” of the heat engine performance. Particularly, in the limit of $\gamma \rightarrow \infty$ with infinite cold reservoir, the tradeoff in Eq. (10) reduces to a concise form $\tilde{P} \leq 4\tilde{\eta}(1 - \tilde{\eta})$.

With the obtained power-efficiency tradeoff, it is straightforward to find the efficiency at an arbitrary given power \tilde{P} being bounded in the region of $\tilde{\eta}_- \leq \tilde{\eta} \leq \tilde{\eta}_+$, where $\tilde{\eta}_{\pm}$ are defined as [35]

$$\tilde{\eta}_{\pm} \equiv 1 - \frac{\lambda\tilde{P}}{(1 \pm \sqrt{1 - \tilde{P}})^2 + \lambda\tilde{P}}. \quad (11)$$

The upper bound $\tilde{\eta}_+$, serving as the maximum efficiency for an arbitrary average power, returns to its counterpart in the infinite-reservoir case by replacing η_{MW} with η_{C} [19,20,23]. Obviously, $\tilde{\eta}_+$ approaches 1 in the quasistatic regime of $\tilde{P} \rightarrow 0$, namely, $\eta \rightarrow \eta_{\text{MW}}$, as shown in Fig. 2.

Efficiency at maximum average power. When the heat engine achieves its maximum average power ($\tilde{P} = 1$), the upper

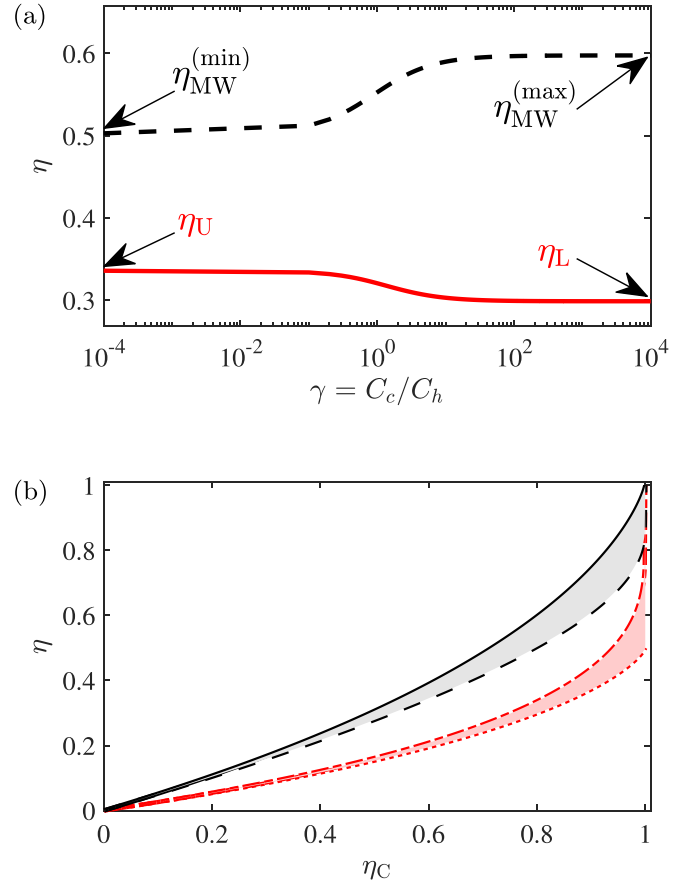


FIG. 3. Dependence of η_{MAP} and η_{MW} on γ and η_{C} . (a) η_{MAP} and η_{MW} as a function of γ . The red solid curve and black dashed curve represent η_{MAP} and η_{MW} , respectively. In this example, $\eta_{\text{C}} = 0.8$. (b) η_{MAP} and η_{MW} as a function of η_{C} . The upper (lower) bound η_{U} (η_{L}) of η_{MAP} in Eq. (13) is plotted as the red dash-dotted (dotted) curve; the (light red) area between the dash-dotted curve and dotted curve is the available range of η_{MAP} . The upper (lower) bound of η_{MW} is represented by the black solid (dashed) curve, and the (gray) area between the solid curve and dashed curve is the achievable range of η_{MW} .

and lower bound in Eq. (11) converge to the EMAP:

$$\eta_{\text{MAP}} = \frac{\eta_{\text{MW}}}{2 - \eta_{\text{MW}}/(1 + \gamma)}, \quad (12)$$

which is a monotonically decreasing function of γ as shown by the red solid curve in Fig. 3(a). In contrast, η_{MW} (black dashed curve) increases with γ monotonically [34]. The upper bound (η_{U}) and lower bound (η_{L}) of η_{MAP} satisfy

$$\eta_{\text{L}} \equiv \frac{\eta_{\text{MW}}^{(\max)}}{2} \leq \eta_{\text{MAP}} \leq \frac{\eta_{\text{MW}}^{(\min)}}{2 - \eta_{\text{MW}}^{(\min)}} \equiv \eta_{\text{U}}, \quad (13)$$

where $\eta_{\text{MW}}^{(\max)} \equiv \eta_{\text{MW}}(\gamma \rightarrow \infty)$ and $\eta_{\text{MW}}^{(\min)} \equiv \eta_{\text{MW}}(\gamma = 0)$. As the result of the opposite monotonicity, there exists a competitive relation between η_{MAP} and η_{MW} . Namely, η_{MAP} achieves its maximum even when η_{MW} is minimum in the limit $\gamma \rightarrow 0$, and vice versa. The lower bound of this general EMAP recovers the result obtained in the special case with infinite large cold reservoir [29]. In addition, for the symmetric case ($\gamma = 1$) demonstrated in Fig. 2, $\eta_{\text{MW}} = \eta_{\text{CA}}$ and

$\eta_{\text{MAP}} = 2\eta_{\text{CA}}/(4 - \eta_{\text{CA}})$. Here $\eta_{\text{CA}} \equiv 1 - \sqrt{T_c^{[i]}/T_h^{[i]}}$ is the Curzon-Ahlborn efficiency [7–10] determined by the initial temperatures of the reservoirs.

Figure 3(b) shows the dependence of η_{MAP} on η_C , where the (light red) area between η_U (red dash-dotted curve) and η_L (red dotted curve) is the available range of η_{MAP} . In comparison, the achievable range of η_{MW} is represented with the (gray) area between the black solid curve and the black dashed curve. As demonstrated in this figure, in the small- η_C regime, there exist γ -independent scalings for η_{MAP} and η_{MW} . Such universalities can be explicitly obtained by expanding η_{MAP} and η_{MW} with respect to η_C :

$$\eta_{\text{MW}} = \frac{1}{2}\eta_C + \frac{1}{6}\left(1 - \frac{1/2}{\gamma + 1}\right)\eta_C^2 + O(\eta_C^3), \quad (14)$$

$$\eta_{\text{MAP}} = \frac{1}{4}\eta_C + \frac{1}{12}\left(1 + \frac{1/4}{\gamma + 1}\right)\eta_C^2 + O(\eta_C^3). \quad (15)$$

Obviously, the first-order coefficients of both η_{MW} and η_{MAP} are independent of the heat capacity ratio γ , as we inferred from Fig. 3(b). Up to the first order of η_C , the universality of η_{MAP} scales as $\eta_{\text{MAP}} \sim \eta_C/4$. Meanwhile, the universality of η_{MW} follows as $\eta_{\text{MW}} \sim \eta_C/2$, which has also been revealed in previous studies [33,34]. Nevertheless, the coefficients corresponding to the second order of η_C are γ dependent for η_{MAP} and η_{MW} . The signs of the terms containing γ in η_{MAP} and η_{MW} are opposite, which is consistent with the opposite monotonicity of η_{MAP} and η_{MW} (with respect to γ).

Optimal operation protocol of the heat engine. As a process function, the path dependence of entropy production σ in the parameter space makes it rely on the control protocol applied to the working substance [43,44]. Therefore, the efficiency and power of the heat engine are inseparable from the specific operation protocol of the cycle. To achieve the boundary of the tradeoff (10) or the EMAP (12), we demonstrate the optimal operation of the heat engine associated with the minimal entropy production σ_{min} with a specific example. For a finite-time Carnot heat engine the working substance of which is the ideal gas with volume V (control parameter), the minimal entropy production condition, i.e., $\dot{Q}_h = \sqrt{L_{22}\Sigma_{\text{min}}}/\tau$, allows us to find the optimal control protocol for $V(t)$ from the energy conservation relation of the gas [35].

The optimal operation protocol of the heat engine is shown in Fig. 4, where A (C) represents the finite-time isothermal expansion (compression) process with duration $t_h^{(m)}$ ($t_c^{(m)}$) in the m th ($m = 1, 2, 3, \dots, M$) cycle. During the isothermal expansion (compression), the gas volume changes exponentially with time as $V_h^{(m)}(\tilde{t}) = V_{h,i}^{(m)} \exp(\Gamma_h^{(m)}\tilde{t})$ [$V_c^{(m)}(t') = V_{c,i}^{(m)} \exp(-\Gamma_c^{(m)}t')$] with $\tilde{t} \equiv t - (m-1)\tau_c$ [$t' \equiv t - (m-1)\tau_c - t_h^{(m)}$]. Here, the initial volume of the gas in the isothermal expansion process $V_{h,i}^{(m)} = V_{h,i}$ is fixed in each cycle, while the initial volumes of the other three processes ($V_{h,f}^{(m)}$, $V_{c,i}^{(m)}$, and $V_{c,f}^{(m)}$) are determined by the full operation protocol. $\Gamma_{h(c)}^{(m)}$ represents the isothermal expansion (compression) rate of the m th cycle [35]. The adiabatic equation of ideal gas is satisfied in the adiabatic processes B and D, the duration of which is

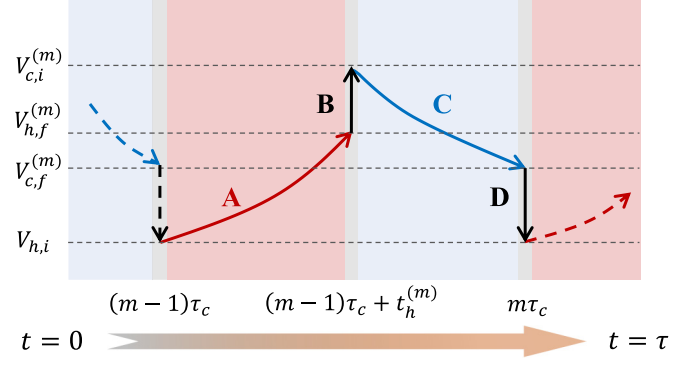


FIG. 4. The diagram of the optimal operation protocol of the m th cycle with the control parameter V (gas volume). In the isothermal expansion (expression) process A (C) of duration t_h (t_c), V changes exponentially with time, while in adiabatic processes (B and D) V is quenched with the adiabatic equation of ideal gas being satisfied.

ignored in comparison with that of the isothermal processes [15,44,45]. It is worth mentioning that a recent study [46] obtained similar optimal operation to realize the efficiency at maximum power of a Brownian heat engine between constant temperature reservoirs. This reminds us that such an optimal operation scheme may be universal for some types of finite-time heat engines.

Conclusion and discussion. In summary, we successfully obtained a general power-efficiency tradeoff for heat engines operating between two finite-sized reservoirs within the linear response regime. With such a tradeoff, we showed the achievable range of efficiency for a given average power, and the universal efficiency at maximum average power. To achieve the optimal performance of the heat engine, corresponding to the boundary of the power-efficiency tradeoff, the optimal operation protocol of an ideal gas heat engine is demonstrated. The predicted results can be tested on some state-of-art platforms [44,47]. Moreover, by replacing η_{MW} with η_C , some typical constraints in the finite case become their corresponding counterparts in the infinite case. These thermodynamic constraints specify the full operation regime of the heat engines in real-world circumstances. This paper paves the way for the joint optimization of the thermodynamic cycle by adjusting the ratio of the heat capacities of the reservoirs and controlling the operation of the cycle, and may shed light on investigating the irreversibility of nonequilibrium thermodynamic processes off the thermodynamic limit.

The temperature-dependent feature of the reservoir's heat capacity [33], the quantumness of the reservoir [48–50], the deviation of entropy production from $1/\tau$ scaling beyond the slow-driving regime [23,43,44,51], and the fluctuations in heat engine performance [52–54] are expected to be taken into future considerations.

Acknowledgments. We thank G. H. Dong and Y. Chen for helpful suggestions. We are grateful to the anonymous referees for enlightening comments. This work is supported by the National Natural Science Foundation of China (Grants No. 12088101, No. U1930402, and No. U1930403). Y.-H. Ma acknowledges support from the China Postdoctoral Science Foundation (Grant No. BX2021030).

- [1] K. Huang, *Introduction To Statistical Physics*, 2nd ed. (CRC, Boca Raton, FL, 2013).
- [2] B. Andresen, R. S. Berry, M. J. Ondrechen, and P. Salamon, *Acco. Chem. Res.* **17**, 266 (1984).
- [3] U. Seifert, *Rep. Prog. Phys.* **75**, 126001 (2012).
- [4] V. Holubec and A. Ryabov, *Phys. Rev. E* **96**, 062107 (2017).
- [5] R. Kosloff, *J. Chem. Phys.* **150**, 204105 (2019).
- [6] Z.-C. Tu, *Front. Phys.* **16**, 1 (2021).
- [7] J. Yvon, in *Proceedings of the First Geneva Conference*, 1955 (unpublished).
- [8] P. Chambadal, *Les Centrales Nuclaires* (Armand Colin, France, 1957), Chap. 3.
- [9] I. I. Novikov, *J. Nucl. Energy* (1954) **7**, 125 (1958).
- [10] F. L. Curzon and B. Ahlborn, *Am. J. Phys.* **43**, 22 (1975).
- [11] C. Van den Broeck, *Phys. Rev. Lett.* **95**, 190602 (2005).
- [12] Y. Izumida and K. Okuda, *Europhys. Lett.* **83**, 60003 (2008).
- [13] T. Schmiedl and U. Seifert, *Europhys. Lett.* **83**, 30005 (2008).
- [14] Z. C. Tu, *Journal Phys. A: Math. Theor.* **41**, 312003 (2008).
- [15] M. Esposito, R. Kawai, K. Lindenberg, and C. Van den Broeck, *Phys. Rev. Lett.* **105**, 150603 (2010).
- [16] Y. Wang and Z. C. Tu, *Phys. Rev. E* **85**, 011127 (2012).
- [17] C. V. D. Broeck, *Europhys. Lett.* **101**, 10006 (2013).
- [18] V. Holubec and A. Ryabov, *Phys. Rev. E* **92**, 052125 (2015).
- [19] V. Holubec and A. Ryabov, *J. Stat. Mech.: Theo. Exp.* (2016) 073204.
- [20] R. Long and W. Liu, *Phys. Rev. E* **94**, 052114 (2016).
- [21] N. Shiraishi, K. Saito, and H. Tasaki, *Phys. Rev. Lett.* **117**, 190601 (2016).
- [22] V. Cavina, A. Mari, and V. Giovannetti, *Phys. Rev. Lett.* **119**, 050601 (2017).
- [23] Y.-H. Ma, D. Xu, H. Dong, and C.-P. Sun, *Phys. Rev. E* **98**, 042112 (2018).
- [24] A. C. Barato and U. Seifert, *Phys. Rev. Lett.* **114**, 158101 (2015).
- [25] J. M. Horowitz and T. R. Gingrich, *Phys. Rev. E* **96**, 020103(R) (2017).
- [26] M. J. Ondrechen, B. Andresen, M. Mozurkewich, and R. S. Berry, *Am. J. Phys.* **49**, 681 (1981).
- [27] M. J. Ondrechen, M. H. Rubin, and Y. B. Band, *J. Chem. Phys.* **78**, 4721 (1983).
- [28] H. S. Leff, *Am. J. Phys.* **55**, 701 (1987).
- [29] Y. Izumida and K. Okuda, *Phys. Rev. Lett.* **112**, 180603 (2014).
- [30] Y. Wang, *Phys. Rev. E* **90**, 062140 (2014).
- [31] R. S. Johal, *Phys. Rev. E* **94**, 012123 (2016).
- [32] H. Tajima and M. Hayashi, *Phys. Rev. E* **96**, 012128 (2017).
- [33] Y.-H. Ma, *Entropy* **22**, 1002 (2020).
- [34] R. S. Johal and R. Rai, *Europhys. Lett.* **113**, 10006 (2016).
- [35] See Supplemental Material at <http://link.aps.org/supplemental/10.1103/PhysRevE.105.L022101> for detailed discussion on the reversible regime (Sec. I), the lower bound of irreversible entropy production (Sec. II), the dissipation work and power-efficiency tradeoff (Sec. III), the bounds of $\tilde{\eta}_{\pm}$ (Sec. IV), and the optimal operation of the engine (Sec. V).
- [36] Y. Izumida and K. Okuda, *Phys. Rev. E* **80**, 021121 (2009).
- [37] K. Proesmans and C. Van den Broeck, *Phys. Rev. Lett.* **115**, 090601 (2015).
- [38] Y. Izumida, *Phys. Rev. E* **103**, L050101 (2021).
- [39] G. Ruppeiner, *Phys. Rev. A* **20**, 1608 (1979).
- [40] P. Salamon and R. S. Berry, *Phys. Rev. Lett.* **51**, 1127 (1983).
- [41] G. E. Crooks, *Phys. Rev. Lett.* **99**, 100602 (2007).
- [42] K. Sekimoto and S. ichi Sasa, *J. Phys. Soc. Japan* **66**, 3326 (1997).
- [43] Y.-H. Ma, D. Xu, H. Dong, and C.-P. Sun, *Phys. Rev. E* **98**, 022133 (2018).
- [44] Y.-H. Ma, R.-X. Zhai, J. Chen, C. P. Sun, and H. Dong, *Phys. Rev. Lett.* **125**, 210601 (2020).
- [45] Z.-C. Tu, *Chin. Phys. B* **21**, 020513 (2012).
- [46] Y.-H. Chen, J.-F. Chen, Z. Fei, and H.-T. Quan, [arXiv:2108.04128](https://arxiv.org/abs/2108.04128).
- [47] I. A. Martínez, É. Roldán, L. Dinis, D. Petrov, J. M. R. Parrondo, and R. A. Rica, *Nat. Phys.* **12**, 67 (2015).
- [48] D. Z. Xu, S.-W. Li, X. F. Liu, and C. P. Sun, *Phys. Rev. E* **90**, 062125 (2014).
- [49] J. Roßnagel, O. Abah, F. Schmidt-Kaler, K. Singer, and E. Lutz, *Phys. Rev. Lett.* **112**, 030602 (2014).
- [50] Y.-H. Ma, C. L. Liu, and C. P. Sun, [arXiv:2110.04550](https://arxiv.org/abs/2110.04550).
- [51] Y.-H. Ma, H. Dong, and C. P. Sun, *Commun. Theor. Phys.* **73**, 125101 (2021).
- [52] G. Verley, T. Willaert, C. Van den Broeck, and M. Esposito, *Phys. Rev. E* **90**, 052145 (2014).
- [53] T. Denzler and E. Lutz, *Phys. Rev. Research* **2**, L032062 (2020).
- [54] Z. Fei, J. F. Chen, and Y.-H. Ma, *Phys. Rev. A* **105**, 022609 (2022).